Toward Tradeoff Between Impact Force Reduction and Maximum Safe Speed: Dynamic Parameter Optimization of Variable Stiffness Robots

Siyang Song
Walker Department of Mechanical Engineering,
The University of Texas at Austin,
Austin, TX 78712
e-mail: sysong@utexas.edu

Yu She
Computer Science and Artificial Intelligence Laboratory,
Massachusetts Institute of Technology,
Cambridge, MA 02139
e-mail: yushe@mit.edu

Junmin Wang
Fellow ASME
Walker Department of Mechanical Engineering,
The University of Texas at Austin,
Austin, TX 78712
e-mail: jwang@austin.utexas.edu

Hai-Jun Su
Fellow ASME
Department of Mechanical and Aerospace Engineering,
The Ohio State University,
Columbus, OH 43210
e-mail: su.298@osu.edu

Variable stiffness robots may provide an effective way of trading-off between safety and speed during physical human–robot interaction. In such a compromise, the impact force reduction capability and maximum safe speed are two key performance measures. To quantitatively study how dynamic parameters such as mass, inertia, and stiffness affect these two performance measures, performance indices for impact force reduction capability and maximum speed of variable stiffness robots are proposed based on the impact ellipsoid in this paper. The proposed performance indices consider different impact directions and kinematic configurations in the large. Combining the two performance indices, the global performance of variable stiffness robots is defined. A two-step optimization method is designed to achieve this global performance. A two-link variable stiffness link robot example is provided to show the efficacy of the proposed method. [DOI: 10.1115/1.4046839]

Keywords: variable stiffness robot, impact force reduction, maximum safe speed, dynamic parameter optimization, physical human–robot interaction, dynamics, robot design, soft robots

1 Introduction

With the development of collaborative robots, the physical human–robot interaction (pHRI) draws increasingly intensive attraction in recent years. Safety is always the primary concern in pHRI. To ensure safety, industrial standards such as Ref. [1] restricted the tool-center-point speed to 0.25 m/s, which limited the dynamic power and static space. However, these requirements sacrifice robot speed and efficiency. To have a better tradeoff between the safety and speed, there have been several interesting concepts toward these two goals, ranging from mechanical designs [2–4], controls [5–9], to motion planning [10–12]. Among those approaches, the variable stiffness (VS) concept is promising because it may address both safety and efficiency simultaneously. Designs such as the VS actuator (VSA) and VS link (VSL) have been proposed to improve the safety and speed of pHRI. The basic idea of using a VS robot for pHRI is proposed in Ref. [2]. By varying the stiffness of the robot, two different operating modes are introduced: the stiff-and-slow mode and the fast-and-soft mode. VS robots have a higher natural frequency and less vibration in the stiff-and-slow operation and can achieve a faster speed in the fast-and-soft operation. While an impact between a human and a robot happens in the fast-and-soft operation, part of the robot mass/inertia can be decoupled during the impact [2,13]. Therefore, for the same impact velocity, the VS robots generate smaller impact force compared with traditional rigid robots. This impact reduction effect determines how much benefit we can obtain by using the VS because a larger impact force reduction may allow faster motion in the fast-and-soft operating mode. Based on this two-mode concept, many design approaches are proposed by researchers for both VSA and VSL. In Refs. [2] and [14], the authors discussed a novel VSA design and its application to efficient pHRI. In Ref. [15], an upgraded VSA is developed based on the results in Ref. [14]. The impact test results in Ref. [14] show that a VSA robot can decouple the effective mass/inertia during the impact and generates less acceleration. In Ref. [9], by employing the proposed control and planning methods, a VSL arm can be safer and faster than the traditional robot. In Ref. [16], a novel VSL design is proposed, and Ref. [17] discussed its collision detection and reaction strategies. In Ref. [18], the authors proposed a novel VSL design and discussed the stiffness control. A VSL is designed in Ref. [19] and its stiffness can change up to 17 times, which is promising for pHRI applications. These efforts have shown the benefits of VS robots for pHRI applications from different aspects, such as impact reduction [15,17] and faster work speed [2,9]. However, an important question that has not been answered in these studies is: how do we design the mass and flexibility properties of a VS robot to have significant benefits?

We already know that large impact reduction can let VS robots move faster in the fast-and-soft mode. A heavyweight design may have a significant impact reduction because more mass/inertia can be decoupled during the impact. However, the maximum safe speed is possibly limited by the heavyweight. Thus, there is always a design tradeoff between the impact reduction and the maximum safe speed. A problem at hand is how to optimize the VS robot dynamics (mass/inertia and flexibility) to compromise the two goals (e.g., large impact reduction and maximum safe speed) to maximize the benefits of VS robots. For VS robots, discussions on this problem are still not clear. In Ref. [20], design guidelines for a single-link VSL robot are presented, and it presents how the robot dynamics affect the impact reduction. The single-link case in Ref. [20] is a good start, but several problems are not discussed, such as how kinematic configurations and impact direction affect the impact reduction. For the multi-link case, the dynamic parameter optimization problem for the VS robot is still open.

In this paper, a VS robot dynamic parameter optimization is proposed with measures of the impact force reduction and maximum safe speed. To quantify the impact force reduction of a VS robot, an impact ellipsoid method for the VS robot is introduced in this paper. For a traditional robot with constant stiffness (CS, can be rigid/flexible), the impact ellipsoid is introduced in Ref. [21] to describe how mass/inertial properties, kinematic configurations, and impact direction affect the impact. The concept of impact ellipsoid and its variants have been used in design optimization [3] and

Contributed by the Mechanisms and Robotics Committee of ASME for publication in the Journal of Mechanisms and Robotics. Manuscript received November 25, 2019; final manuscript received March 9, 2020; published online May 11, 2020. Assoc. Editor: Shaoping Bai.

planning [22] for traditional CS robots. For VS robots, flexibility plays an important role in the impact ellipsoid. Using an impact model, we propose an efficient way to calculate the impact ellipsoid for a VS robot with different levels of flexibility. Using the impact ellipsoid, the performance (impact force reduction and maximum safe speed) of a VS robot can be evaluated over the entire workspace. Furthermore, the performance is optimized by tuning the dynamics of the VS robot (mass/inertia and flexibility). The kinematic design optimization is not discussed in this paper because the design goals for kinematic such as dexterity and workspace are not the foci of this work. Readers can refer to Refs. [23,24] about the kinematic optimization.

In Sec. 2, preliminaries including the impact ellipsoid and the impact model are introduced. Measures of impact force reduction and maximum safe speed are introduced based on the impact ellipsoid. In Sec. 3, the design optimization is introduced. In Sec. 4, a two-link VSL example is presented to validate the proposed design optimization method. Conclusions are given in Sec. 5.

2 Preliminaries

2.1 Measure of the Impact Force. Researchers have used quite a few criteria for evaluating the impact between a human and a robot. Some popular criteria include the Head Injury Criterion (HIC) [25], the maximum power index (MPI) [26], the Gadd Severity Index (GSI) [27], and the maximum impact force (MIF) [13]. HIC, MPI, and GSI were firstly proposed for the automotive industry and then introduced to pHRI research. These three criteria are defined based on acceleration. However, for many possible injuries in pHRI, such as fracturing of skins and bones, the impact force is a better measure [3,13]. In this paper, we will use MIF as the safety criterion to derive the impact ellipsoid and visualize the maximum safe speed. Based on a mass–spring–mass model, the analytical solution of the MIF is as follows [28]:

$$F_{\max} = v_c\sqrt{k_c\frac{m_H m_R}{m_H + m_R}} \tag{1}$$

where m_H is the human effective mass, m_R is the robot effective mass, k_c is the contact stiffness (covering material), and v_c is the impact velocity. The effective mass m_R is related to the kinematic configurations and the impact direction. For traditional rigid robots, the dynamics of the robot can be described by the following Euler–Lagrange equation [29]

$$M_{rig}(\mathbf{q}_{rig})\ddot{\mathbf{q}}_{rig} + C_{rig}(\mathbf{q}_{rig}, \dot{\mathbf{q}}_{rig})\dot{\mathbf{q}}_{rig} + \mathbf{G}_{rig}(\mathbf{q}_{rig}) = \boldsymbol{\tau} \tag{2}$$

where $\mathbf{q}_{rig}$ is the vector of joint displacements. M_{rig}, C_{rig}, and $\mathbf{G}_{rig}$ are the inertia matrix, centrifugal and Coriolis matrix, and gravity vector, respectively. $\boldsymbol{\tau}$ is the motor torque vector. In Ref. [30], the effective mass m_R is given by the following equation

$$\frac{1}{m_R(\mathbf{q}_{rig}, u)} = \mathbf{u}J_{rig}(\mathbf{q}_{rig})M_{rig}^{-1}(\mathbf{q}_{rig})J_{rig}^{T}(\mathbf{q}_{rig})\mathbf{u}^T \tag{3}$$

where $\mathbf{u}$ is the unit row vector along with the impact direction and $J_{rig}(\mathbf{q}_{rig})$ is the Jacobian matrix. To investigate the effective mass in different impact directions, the effective mass ellipsoid [30] can be defined by

$$\mathbf{z}J_{rig}(\mathbf{q}_{rig})M_{rig}^{-1}(\mathbf{q}_{rig})J_{rig}^{T}(\mathbf{q}_{rig})\mathbf{z}^T = 1 \tag{4}$$

the direction of the row vector $\mathbf{z}$ is the impact direction and the magnitude of $\mathbf{z}$ is $\sqrt{m_R(\mathbf{q}_{rig}, \mathbf{z}/\|\mathbf{z}\|)}$.

To visualize the maximum impact force (1), rewrite Eq. (1) by substituting Eq. (3) into it

$$\begin{aligned} F_{\max} &= v_c\sqrt{k_c\frac{m_H m_R}{m_H + m_R}} = v_c\sqrt{k_c\frac{m_H}{m_H/m_R + 1}} \\ &= v_c\sqrt{\frac{k_c m_H}{m_H\mathbf{u}J_{rig}(\mathbf{q}_{rig})M_{rig}^{-1}(\mathbf{q}_{rig})J_{rig}^{T}(\mathbf{q}_{rig})\mathbf{u}^T + \mathbf{u}\mathbf{u}^T}} \\ &= v_c\sqrt{\frac{k_c m_H}{\mathbf{u}[m_H J_{rig}(\mathbf{q}_{rig})M_{rig}^{-1}(\mathbf{q}_{rig})J_{rig}^{T}(\mathbf{q}_{rig}) + I_{3\times3}]\mathbf{u}^T}} \end{aligned} \tag{5}$$

where $I_{3\times3}$ is a 3-by-3 identity matrix. Note that in Eqs. (1) and (5), we have a velocity-independent term. Define the local impact strength by this velocity-independent term

$$\sigma(\mathbf{q}_{rig}, \mathbf{u}) = \sqrt{\frac{k_c m_H}{\mathbf{u}[m_H J_{rig}(\mathbf{q}_{rig})M_{rig}^{-1}(\mathbf{q}_{rig})J_{rig}^{T}(\mathbf{q}_{rig}) + I_{3\times3}]\mathbf{u}^T}} \tag{6}$$

It can be visualized by the impact ellipsoid as follows:

$$\begin{aligned} &\mathbf{z}\Lambda\mathbf{z}^T = k_c m_H \\ &\Lambda = m_H J_{rig}(\mathbf{q}_{rig})M_{rig}^{-1}(\mathbf{q}_{rig})J_{rig}^{T}(\mathbf{q}_{rig}) + I_{3\times3} \end{aligned} \tag{7}$$

where the magnitude of $\mathbf{z}$ is $\sigma(\mathbf{q}_{rig}, \mathbf{z}/\|\mathbf{z}\|)$. The directions of the three principal semi-axes of the impact ellipsoid correspond to the three eigenvectors of Λ. Lengths of the three principal semi-axes are $\sqrt{k_c m_H/\lambda_{\Lambda,i}}$, and $\lambda_{\Lambda,i}$, $i = 1, 2, 3$ are three eigenvalues of Λ. The overall impact strength for certain kinematic configuration can be defined by the volume of the ellipsoid, which is

$$\mu(\mathbf{q}_{rig}) = \frac{4}{3}\pi\prod_{i=1}^{3}\sqrt{k_c m_H/\lambda_{\Lambda,i}} \tag{8}$$

It should be noted that the volume is just one of the possible measures to represent the overall impact strength.

2.2 Measure of the Impact Force Reduction. For VS robots, the dynamics are different from Eq. (2). Typically, the dynamics of the flexible robots, including the flexible joint (FJ) robots [31] and flexible link robots [32,33], can be denoted by the following Euler–Lagrange equation:

$$\begin{aligned} &M_{VS}(\mathbf{q})\ddot{\mathbf{q}} + C_{VS}(\mathbf{q}, \dot{\mathbf{q}})\dot{\mathbf{q}} + K_{VS}\mathbf{q} + \mathbf{G}_{VS}(\mathbf{q}) = \boldsymbol{\tau}_{VS} \\ &\boldsymbol{\tau}_{VS} = \begin{pmatrix} \boldsymbol{\tau}_m \\ \mathbf{0}_{n\times1} \end{pmatrix} \end{aligned} \tag{9}$$

where $\mathbf{q} = (\boldsymbol{\theta}^T, \boldsymbol{\eta}^T)^T$ is a column vector. Here, $\boldsymbol{\theta}$ is the m-dimensional column vector of the joint displacements and $\boldsymbol{\eta}$ is the n-dimensional column vector of the generalized coordinates of flexibility. $\boldsymbol{\eta}$ can be the FJ displacements for VSA robots or the modal coordinates for VSL robots (using the assumed mode method). $M_{VS}(\mathbf{q})$ is the $k\times k$ inertia matrix where $k = m + n$. $C_{VS}(\mathbf{q}, \dot{\mathbf{q}})$ is a $k\times k$ matrix, and it includes the Coriolis and centrifugal terms. $\mathbf{G}_{VS}(\mathbf{q})$ is the k-dimensional gravity column vector. K_{VS} is the $k\times k$ stiffness matrix. $\boldsymbol{\tau}_{VS}$ is the k-dimensional input vector. $\boldsymbol{\tau}_m$ is the m-dimensional vector of motor torque, and $\mathbf{0}_{n\times1}$ is the n-dimensional zero vector.

Different from the dynamics of the traditional rigid robots in Eq. (2), the stiffness term $K_{VS}\mathbf{q}$ affects the impact force. To investigate the impact reduction capability, let us consider two extreme setups for the stiffness matrix K_{VS}. When the stiffness of the robot is infinitely large (i.e., the robot is rigid), the dynamics of the VS robot will degenerate to an equation similar to Eq. (2)

$$M_{rig}(\boldsymbol{\theta})\ddot{\boldsymbol{\theta}} + C_{rig}(\boldsymbol{\theta}, \dot{\boldsymbol{\theta}})\dot{\boldsymbol{\theta}} + \mathbf{G}_{rig}(\boldsymbol{\theta}) = \boldsymbol{\tau} \tag{10}$$

In the dynamic equation (10), the flexibility $\boldsymbol{\eta}$ and stiffness matrix

K_{VS} are absent from the equation and only $\boldsymbol{\theta}$ is left. Then, the impact ellipsoid can be derived as follows:

$$\begin{aligned} &\mathbf{z}\Lambda_{rig}\mathbf{z}^T = k_c m_H \\ &\Lambda_{rig} = m_H J_{rig}(\boldsymbol{\theta}) M_{rig}^{-1}(\boldsymbol{\theta}) J_{rig}^T(\boldsymbol{\theta}) + I_{3\times 3} \end{aligned} \tag{11}$$

When the stiffness of the robot goes to zero, the dynamics (9) will degenerate to the following equation:

$$M_{VS}(\mathbf{q})\ddot{\mathbf{q}} + C_{VS}(\mathbf{q}, \dot{\mathbf{q}})\dot{\mathbf{q}} + \mathbf{G}_{VS}(\mathbf{q}) = \boldsymbol{\tau}_{VS} \tag{12}$$

Compared with Eq. (2), Eq. (12) is also a rigid robot but with redundancies brought by flexibility. Based on Eq. (12), another impact ellipsoid can be derived in a similar way

$$\begin{aligned} &\mathbf{z}\Lambda_{soft}\mathbf{z}^T = k_c m_H \\ &\Lambda_{soft} = m_H J_{VS}(\bar{\mathbf{q}}) M_{VS}^{-1}(\bar{\mathbf{q}}) J_{VS}^T(\bar{\mathbf{q}}) + I_{3\times 3} \\ &\bar{\mathbf{q}} = (\boldsymbol{\theta}^T, \mathbf{0}_{1\times n})^T \end{aligned} \tag{13}$$

Note that the flexible deformation coordinates $\boldsymbol{\eta}$ are set to be zero in $\bar{\mathbf{q}}$. The kinematic configuration only considers the motor displacements. J_{VS} is the Jacobian matrix of the VS robot. These two ellipsoids, $\mathbf{z}\Lambda_{rig}\mathbf{z}^T = k_c m_H$ and $\mathbf{z}\Lambda_{soft}\mathbf{z}^T = k_c m_H$, have the same center but different volumes. Figure 1 illustrates the two impact ellipsoids.

The impact force reduction of the two extreme setups (stiffness being zero and infinity) can be intuitively defined by the difference between the volumes of the two ellipsoids

$$\Delta\mu(\boldsymbol{\theta}) = \mu_{rig}(\boldsymbol{\theta}) - \mu_{soft}(\boldsymbol{\theta}) \tag{14}$$

In Fig. 1, $\Delta\mu_{\max}$ represents the area between the two solid ellipses. In practice, instead of changing from zero to infinity, many VS designs only change the flexibility within a range of $[K_{min}, K_{\max}]$, and impact force reduction actually is the area between the two dash-line ellipsoids in Fig. 1.

For impact ellipsoids with a stiffness matrix, derivations from Eq. (2) to Eq. (7) are invalid because the dynamics now involve the stiffness matrix. From Eqs. (1) and (5), we know

$$F_{\max}(\boldsymbol{\theta}, \mathbf{u}, K_{VS}) = v_c \sigma(\boldsymbol{\theta}, \mathbf{u}, K_{VS}) \tag{15}$$

and the impact strength can be calculated by

$$\sigma(\boldsymbol{\theta}, \mathbf{u}, K_{VS}) = \frac{F_{\max}(\boldsymbol{\theta}, \mathbf{u}, K_{VS})}{v_c} \tag{16}$$

The v_c can be obtained by $v_c = \mathbf{u}J_{VS}(\bar{\mathbf{q}})\dot{\bar{\mathbf{q}}}$. To estimate $F_{max}(\boldsymbol{\theta}, \mathbf{u}, K_{VS})$, we propose a new impact model. Based on Eq. (9),

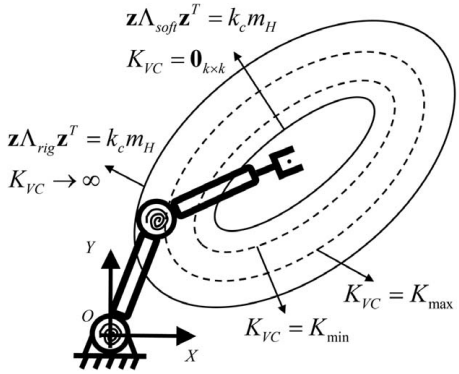

Fig. 1 Impact ellipsoid of the end effector (2D case of a two-link VSA robot)

the impact model can be described by the following equations:

$$\begin{cases} M_{VS}(\mathbf{q})\ddot{\mathbf{q}} + C_{VS}(\mathbf{q}, \dot{\mathbf{q}})\dot{\mathbf{q}} + K_{VS}\mathbf{q} + \mathbf{G}_{VS}(\mathbf{q}) = \boldsymbol{\tau}_{VS} + \boldsymbol{\tau}_{impact} \\ -J_{VS}(q)\boldsymbol{\tau}_{impact} = k_c \mathbf{u}(\mathbf{x}_R - \mathbf{x}_H)\mathbf{u}^T \\ m_H \ddot{\mathbf{x}}_H = k_c \mathbf{u}(\mathbf{x}_R - \mathbf{x}_H)\mathbf{u}^T \end{cases} \tag{17}$$

where $\mathbf{x}_R$ and $\mathbf{x}_H$ are position vectors of the robot and the human in Cartesian space, respectively. F_{impact} and $\boldsymbol{\tau}_{impact}$ are the impact force and impact torque acted on the robot, respectively. By assuming the changes of joint positions are small during the impact, $M_{VS}(\mathbf{q})$, $\mathbf{G}_{VS}(\mathbf{q})$, and $J_{VS}(\mathbf{q})$ are constant during the impact. Furthermore, we have $\mathbf{x}_R = \mathbf{x}_{R,0} + J(\mathbf{q})(\mathbf{q} - \mathbf{q}_0)$, where $\mathbf{x}_{R,0}$ and $\mathbf{q}_0$ are the initial position of the impact point on the robot and the initial joint position, respectively. Also, because the inertia and stiffness matrices dominate the impact, we assume that the motor torque, centrifugal, and Coriolis terms are constant. By these assumptions we made, the nonlinear terms are considered as constants and the impact dynamics is linearized as follows:

$$\begin{cases} M_{VS}(\mathbf{q}_0)\ddot{\mathbf{q}} + K_{VS}\mathbf{q} + C_{VS}(\mathbf{q}_0, \dot{\mathbf{q}}_0)\dot{\mathbf{q}}_0 + \mathbf{G}_{VS}(\mathbf{q}_0) = \boldsymbol{\tau}_{VS} + \boldsymbol{\tau}_{impact} \\ -J_{VS}(\mathbf{q}_0)\boldsymbol{\tau}_{impact} = k_c \mathbf{u}(\mathbf{x}_{R,0} + J_{VS}(\mathbf{q}_0)(\mathbf{q} - \mathbf{q}_0) - \mathbf{x}_H)\mathbf{u}^T \\ m_H \ddot{\mathbf{x}}_H = k_c \mathbf{u}(\mathbf{x}_{R,0} + J_{VS}(\mathbf{q}_0)(\mathbf{q} - \mathbf{q}_0) - \mathbf{x}_H)\mathbf{u}^T \end{cases} \tag{18}$$

Using Eq. (18), we can predict $F_{\max}$ with different $\mathbf{q}$, $\mathbf{u}$, and K_{VS}. To estimate the impact ellipsoid, only $F_{\max}$ in the directions of the three principal semi-axes need to be estimated. Similar to Eq. (8), the impact strength can be estimated and defined by

$$\mu(\boldsymbol{\theta}, K_{VS}) = \frac{4}{3}\pi \prod_{i=1}^{3} \frac{F_{\max,i}(\boldsymbol{\theta}, K_{VS})}{v_{c,i}} \tag{19}$$

where the subscript $i$represents the ith eigendirection.

2.3 Measure of Maximum Safe Speed. With a given safety criterion, $F_{\max} \le F_{crit}$, the maximum permissible velocity can be obtained by

$$v_{crit} = F_{crit}/\sigma \tag{20}$$

Recall the impact ellipsoid (7), the v_{crit} can be visualized by

$$\begin{aligned} &\mathbf{z}\Lambda^{-1}\mathbf{z}^T = \frac{F_{crit}^2}{k_c m_H} \\ &\Lambda = m_H J_{VS}(\bar{\mathbf{q}}) M_{VS}^{-1}(\bar{\mathbf{q}}) J_{VS}^T(\bar{\mathbf{q}}) + I_{3\times 3} \end{aligned} \tag{21}$$

The lengths of the three principal semi-axes correspond to the maximum permissible velocities in three eigen directions, and they are

$$v_{crit,i} = \frac{F_{crit}}{\sqrt{k_c m_H/\lambda_{\Lambda,i}}}, \quad i = 1, 2, 3 \tag{22}$$

Similar to Eq. (8), the overall maximum safe speed can be defined by the volume of the ellipsoid

$$\xi(\boldsymbol{\theta}) = \frac{4}{3}\pi \prod_{i=1}^{3} v_{crit,i} \tag{23}$$

In this section, we introduced how to evaluate the impact force reduction and maximum safe speed by using impact ellipsoid. In Secs. 3–5, design optimization and an example are introduced.

3 Design Optimization

The design optimization problem is how to optimize the dynamics (mass/inertia and flexibility) to maximize the impact force reduction and maximum safe speed over the whole workspace. In this section, we propose a two-step design optimization method to address this problem.

The maximum impact force reduction capability $\Delta\mu$ in Eq. (14) is derived by two dynamic equations (2) and (12). In Eqs. (2) and (12), the stiffness matrix K_{VS} is absent from the equation because the stiffness is either zero or infinity. Therefore, by changing the inertia matrix, the maximum impact force reduction can be designed. In the first step, the inertia matrix is optimized to determine the maximum impact force reduction and the overall maximum safe speed. In this step, the inner bound and outer bound of the impact ellipsoids are designed. In the next step, the stiffness is optimized again to have the maximal impact force reduction within the boundary determined by the first step. In Fig. 1, the two solid ellipsoids are designed in the first step. In the second step, the two dashed ellipses are designed by adjusting the stiffness matrix. Next, we will introduce how to formulate the two-step optimization process.

3.1 Optimization of Mass/Inertial Properties. To consider the impact force reduction and maximum safe speed simultaneously, we combine the impact force reduction $\Delta\mu$ in Eq. (14) and the maximum safe speed ξ in Eq. (23) and propose a compound performance index, which is defined as follows:

$$P(\boldsymbol{\theta}, \Theta_{mass}) = \frac{\Delta\mu(\boldsymbol{\theta}, \Theta_{mass})}{\mu_{rig}(\boldsymbol{\theta}, \Theta_{mass})} + R \cdot \xi_{rig}(\boldsymbol{\theta}, \Theta_{mass}), \quad R > 0 \tag{24}$$

in which, R is a weighting factor. The subscript *rig* represents that the corresponding ellipsoid is derived by dynamics (10). Θ_{mass} are the mass parameters to be designed. The Θ_{mass} can include any to-be-designed mass/inertial parameters not limited to the mass of the link/joint. The first term is the relative impact force reduction, and the second term is related to the maximum safe speed. By adjusting the factor R, the optimization can emphasize the preference of the design (either impact force reduction or maximum safe speed). The performance index (24) is a local performance. It is important to remember that the weighted summation (24) is not the only way to define the compound performance of impact force reduction and maximum safe speed. To consider the global performance over the whole workspace, the global performance index is defined based on Eq. (24)

$$GP_{mass}(\Theta_{mass}) = \frac{\int_W P(\boldsymbol{\theta}, \Theta_{mass}) dW}{\int_W dW}, \quad \boldsymbol{\theta} \in W \tag{25}$$

where W is the workspace. In practice, the index can be calculated by a numerical integration. By maximizing the GP_{mass}, the optimal design parameters Θ^*_{mass} can be found. With Θ^*_{mass}, the inner bound and the outer bound of the impact ellipsoids can be determined. The flexibility can be optimized within the boundary to maximize the impact force reduction further.

3.2 Optimization of Flexibility. In the first step, the mass parameters Θ^*_{mass} are designed to maximize GP_{mass}. For those designs with an infinite stiffness range (zero to infinity), such as Ref. [34], the optimization of flexibility is unnecessary and the mass optimization can finalize the design. However, many other designs have limited capability of changing flexibility. Regardless of different design concepts for a single VSA joint or VSL link, this capability is usually specified by the stiffness ratio of maximum stiffness to minimum stiffness. Even with the same stiffness ratio, different stiffness ranges may have different impact force reduction effects. Therefore, in the second step, the absolute flexibility range with a certain stiffness ratio is optimized to maximize the impact force reduction.

We assume the ratio $\alpha_i = k_{\max,i}/k_{\min,i}$, $i = 1, \ldots, n$ is given. Here, $k_{\max,i}$ and $k_{\min,i}$ are the maximal stiffness and the minimal stiffness for ith VSA/VSL. Because $k_{\max,i} = \alpha_i k_{\min,i}$, the stiffness parameters to be determined are related to $k_{\min,i}$ only. For notation convenience, the stiffness parameters to be optimized are denoted by Θ_{stiff}. The stiffness matrix of the softest configuration and the most rigid configuration can be denoted by $K_{\min}(\Theta_{stiff})$ and $K_{\max}(\Theta_{stiff})$. In $K_{\min}$, the stiffness of each VSA/VSL is the minimal value $k_{\max,i}$. Similarly, for $K_{\max}$, the stiffness of each VSA/VSL is its maximal value $k_{\max,i} = \alpha \cdot k_{\min,i}$.

As we discussed in Secs. 1 and 2, the mass/inertial properties play an important role in the tradeoff between the impact force reduction and the maximum safe speed. For this reason, the mass properties have been optimized. But the impact force reduction can still be small if the range of the flexibility is not proper. In this step, the optimization only considers the impact force reduction. The maximum safe speed is not considered in the flexibility optimization because no matter how we choose the flexibility, the maximum safe speed will not exceed the bound determined by the optimal mass/inertial properties, which is $\xi_{rig}(\boldsymbol{\theta}, \Theta^*_{mass})$. The relative impact force reduction is defined by

$$\Delta\gamma(\Theta_{stiff}, \boldsymbol{\theta}) = \frac{\mu_{\max}(K_{\max}(\Theta_{stiff}), \boldsymbol{\theta}) - \mu_{\min}(K_{\min}(\Theta_{stiff}), \boldsymbol{\theta})}{\mu_{\max}(K_{\max}(\Theta_{stiff}), \boldsymbol{\theta})} \tag{26}$$

where $\mu_{\max}$ and $\mu_{\min}$ are estimated by the impact model (18) and (19). The global reduction is defined as

$$GP_{stiff}(\Theta_{stiff}) = \frac{\int_W \Delta\gamma(\Theta_{stiff}, \boldsymbol{\theta}) dW}{\int_W dW}, \quad \boldsymbol{\theta} \in W \tag{27}$$

By maximizing GP_{stiff}, the optimal stiffness range $[k_{\min,i}, k_{\max,i}]$ for each VSA/VSL can be found. Once again, Eqs. (26) and (27) are not the only way to define the flexibility optimization problem. By changing the performance index, the design can emphasize different aspects.

4 Example

As we discussed in Sec. 2.2, the dynamics of the VSA robot and VSL robot both can be denoted by the Euler–Lagrange equation (9). However, the modeling of the VSL robot is more complicated than the VSA. Because the general coordinates for the flexibility of the VSL robot are derived from a modal analysis, we present a two-link VSL robot example to illustrate the design optimization. The design procedure also works for the VSA robot except for the modeling part.

4.1 Two-Link Variable Stiffness Link Robot. Figure 2 illustrates the coordinates of the two-link VSL robot.

In this example, the lengths of the links, the mass of the payload, and the mass/inertia of the two joints are given. The design problem is to optimize the mass values of the two links and the stiffness range to achieve the optimal impact force reduction and maximum safe speed.

The dynamics of the VSL robots can be modeled by the assumed mode method. The modeling of the VSL robots can be referred to

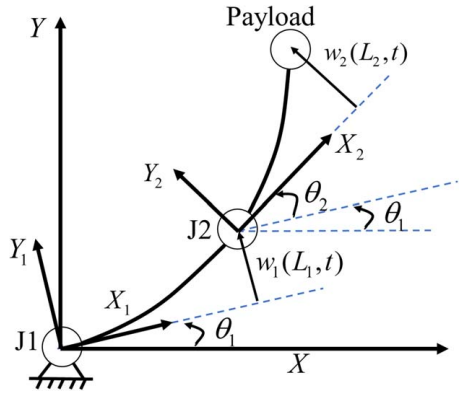

Fig. 2 Two-link flexible link robot

Refs. [33] and [35]. Assuming a relatively small deflection of the link, then the deflection of the ith link at l_i along the coordinateX_i-Y_i can be described by the following equation

$$w_i(l_i, t) = \sum_{j=1}^{\infty} \phi_{ij}(l_i)\eta_{ij}(t), \quad i = 1, 2 \tag{28}$$

where the subscript i is the index of the link, $\phi_{ij}(x)$ is the modal shape function of the jth mode, and $\eta_{ij}(t)$ is the modal coordinate of the$j$th mode. The modal shape function $\phi_{ij}(x)$ can be determined by the clamp-free boundary conditions [36]. In this example, we only consider the first and second modes. ϕ_1, ϕ_2 and η_1, η_2 are the modal shape functions and coordinates for the first and the second modes of link 1. ϕ_3, ϕ_4 and η_3, η_4 are the modal shape functions and coordinates for the first and the second modes of link 2. If we select the modal coordinates as the deflection of each mode at the tip and considering the first two modes of each link, then Eq. (28) can be rewritten as

$$\begin{aligned} w_1(l_1, t) &= \sum_{j=1}^{2} \frac{\phi_j(l_1)}{\phi_j(L_1)}\eta_j(t) \\ w_2(l_2, t) &= \sum_{j=3}^{4} \frac{\phi_j(l_2)}{\phi_j(L_2)}\eta_j(t) \end{aligned} \tag{29}$$

where L_1 and L_2 are the lengths of link 1 and link 2, respectively. Using Eq. (29) and kinematic in Fig. 2, the kinetic energy and potential energy can be derived. Furthermore, the Lagrange equation can be applied, and the dynamics of the VSL robot can be described by the Euler–Lagrange equation in Eq. (9). The modeling of the VSL is not the focus of this paper. Thus, detailed derivations are omitted in this paper, and the reader can refer to Refs. [33] and [35]. The robot has six DOF in total (two vibration modes for each link and two joints).

In the modeling of the VSL robot, only finite numbers of modes are considered to describe the infinite-dimensional vibration. It is important to mention that a softer link involves more vibration modes compared with a stiffer link. It is tricky to select the number of modes used in the modeling because more modes can improve the accuracy of the model especially when the link is soft while requiring a higher calculation effort. For a VSA robot, the vibration is finite-dimensional and the mode problem will not be a concern.

4.2 Design Optimization Setup. Based on the dynamics of Eq. (9), the two-step design optimization can be performed. For this design, the known parameters are shown in Table 1.

With the given parameters, we will optimize the mass of each link in the first step, those are m_1 and m_2. In the second step, the flexural rigidity range of two links, $[EI_1, \alpha EI_1]$ and $[EI_2, \alpha EI_2]$, are optimized. Note that only the minimum flexural rigidities are optimized, the maximum flexural rigidities are determined by the stiffness ratio and the minimum flexural rigidities.

Table 1 Parameters of the two-link VSL robot design

Parts	Properties	Values
Link 1 and 2	Length (m)	0.2
Joint 1 and 2	Inertia (kg m^2)	0.00025
	Mass (kg)	0.2
Payload	Mass (kg)	0.1
m_H[a]	Mass (kg)	2
k_c[b]	Stiffness (N/m)	5000
F_{crit}[c]	Force (N)	100
Stiffness ratio	α	100

[a]The weight of fragile body parts such as head, hand, and forearm are ranging from 0.4 kg to 5 kg according to Ref. [37].
[b]The contact stiffness is assumed to be the smallest contact stiffness as we found in the literature [2].
[c]The maximum permissible forces for human body parts are ranging from 65 N to 220 N according to Ref. [38].

4.3 The First Step: Mass Optimization. For mass optimization, the design is limited within the range $m_1, m_2 \in [0.2, 10]$ kg. For this example, the mass optimization problem is

$$\begin{aligned} &\arg\max GP_{mass}(m_1, m_2) \\ &\text{subject to: } m_1, m_2 \in [0.2, 10], \quad \theta_1, \theta_2 \in [0, \pi] \end{aligned} \tag{30}$$

To optimize the $GP_{mass}(m_1, m_2)$, we use the *fmincon* function in MATLAB. The *fmincon* function can implement solvers such as the interior-point method and the trust-region method for nonlinear constraint optimization problems. The mass optimization (30) has a tradeoff between the maximum impact force reduction and maximum safe speed which is shown in Fig. 3. In Fig. 3, R is increasing from 0 to 0.1 with 40 different values (three of which are marked). While $R = 0.1$, the design is dominated by the maximum safe speed and mass is minimized ($m_1 = m_2 = 0.2$).

In Fig. 3, the maximum impact force reduction and maximum safe speed indices are defined as follows:

$$\begin{aligned} \text{Maximum impact force reduction index} &= \frac{\int_W \frac{\Delta\mu(\boldsymbol{\theta}, m_1, m_2)}{\mu_{rig}(\boldsymbol{\theta}, m_1, m_2)} dW}{\int_W dW} \\ \text{Maximum safe speed index} &= \frac{\int_W \xi_{rig}(\boldsymbol{\theta}, m_1, m_2) dW}{\int_W dW} \end{aligned} \tag{31}$$

The impact force reduction and maximum safe speed indices are derived from the first term and the second term of Eq. (24), respectively. The maximum impact reduction index is unitless and can be expressed in percentage. The unit of the maximum safe speed index is m^3/s^3. For the three marked R values in Fig. 3, the mass parameters are shown in Table 2.

From the results shown in Fig. 3 and Table 2, it is clear that the weighting factor R compromises the impact force reduction and maximum safe speed indices. Typically, a heavier design has a larger impact force reduction because more mass can be decoupled during the impact. However, the maximum safe speed index of the heavy design is low for safety reasons. By tuning R, we can emphasize different aspects of the design. A large R means the design

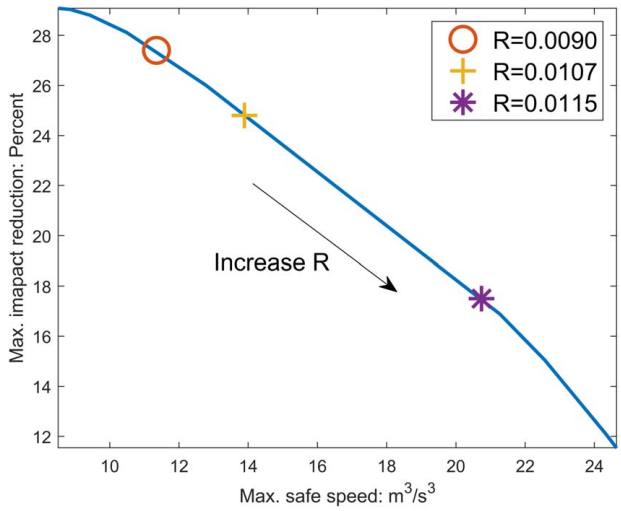

Fig. 3 Tradeoff between maximum impact force reduction and maximum safe speed

Table 2 Mass optimization results

R	$[m_1, m_2]$ (kg)	Max. impact force reduction (%)	Max. safe speed (m^3/s^3)
0.0090	[5.46, 1.01]	27.4	11.35
0.0107	[3.45, 0.62]	24.8	13.89
0.0115	[1.50, 0.20]	17.5	20.74

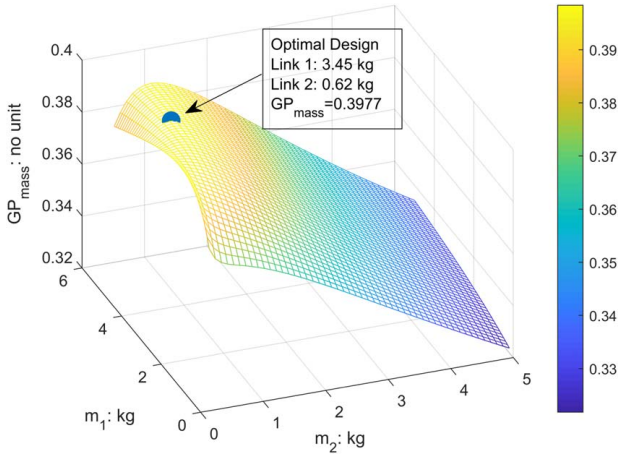

Fig. 4 Mass optimization result ($R = 0.0107$)

focuses more on the maximum safe speed, while a small Rmeans impact force reduction is important. R is usually a small value because the impact force reduction index is significantly smaller than the maximum safe speed index. In this example, we choose the weighting factor $R = 0.0107$ for the final design. The optimization result is illustrated in Fig. 4.

4.4 The Second Step: Flexibility Optimization. Next, the flexural rigidity range is optimized to finalize the design. With the mass parameters being optimized in Sec. 4.3, the reduction index (27) is optimized by tuning the ranges of flexural rigidity of the two links. In this example, the flexibility parameters to be designed are EI_1 and EI_2, which are the smallest flexural rigidities of link 1 and link 2, respectively. For this example, the reduction index (27) now is

$$GP_{stiff}(EI_1, EI_2) = \frac{\int_W \Delta\gamma(EI_1, EI_2, \boldsymbol{\theta})dW}{\int_W dW}, \quad \boldsymbol{\theta} \in W$$

$$\Delta\gamma(EI_1, EI_2, \boldsymbol{\theta}) = \frac{\mu_{\max}(K_{\max}(\alpha EI_1, \alpha EI_2), \boldsymbol{\theta}) - \mu_{\min}(K_{\min}(EI_1, EI_2), \boldsymbol{\theta})}{\mu_{\max}(K_{\max}(\alpha EI_1, \alpha EI_2), \boldsymbol{\theta})} \tag{32}$$

where $\Delta\gamma$ is the relative impact force reduction for a certain kinematic configuration $\boldsymbol{\theta}$. The design optimization is constrained within $EI_1, EI_2 \in [0.1, 50]\text{Pa} \cdot \text{m}^4$. For this example, the optimization problem is

$$\begin{aligned} &\arg\max GP_{stiff}(EI_1, EI_2) \\ &\text{subject to: } EI_1, EI_2 \in [0.1, 50]\text{Pa} \cdot \text{m}^4,\ q_1, q_2 \in [0, \pi] \end{aligned} \tag{33}$$

The result of flexibility optimization is shown in Fig. 5. We use a logarithmic coordinate to show more details when the flexural rigidity is small. In Fig. 5, only the lower bound of the flexural rigidity is shown. The range of the flexural rigidity can be inferred by the stiffness ratio and the lower bound, which is $[EI_{\min}, \alpha EI_{\min}]$.

Compared with the maximum impact force reduction in the first step, which is 24.8%, the impact force reduction after the flexibility optimization is smaller (22.4%) but still significant. If the flexibility is not optimized, the impact force reduction can be insignificant, even with the well-designed mass parameters. For instance, in Fig. 5, when the minimal flexural rigidity of link 2 is greater than $10\ \text{Pa} \cdot \text{m}^4$, the design only has a reduction less than 10%.

4.5 Validations. To validate the design, a VSL simulation model is developed in MATLAB Simscape Multibody. The flexible link is modeled by the finite segment model (FSM) [39]. The impact force is modeled with the Simscape Contact Force Library. The parameters of the model are given in Table 3.

For comparison purposes, a non-optimized (mass and flexibility are not optimized) design and a mass-optimized (only mass is optimized) design are tested. The non-optimized design has the same total mass as the optimal design, while they have different mass distributions. The selection of the unoptimized flexibility refers to several published VSL prototypes [9,19,40]. The minimal flexural rigidity of these prototypes range from 0.5 to $1.2\ \text{Pa} \cdot \text{m}^4$, and we select 0.5 for this simulation because it is the closest value to the optimal design. The three designs are modeled in Simscape by the FSM.

To validate the design, impact simulations with different configurations are conducted. Each design is tested with four different kinematic configurations. For each configuration, the impact ellipsoids for the minimum flexural rigidity and the maximum flexural rigidity are derived from the simulation. To derive the impact ellipsoid, the maximum impact force is simulated and then the ellipsoid is calculated by $\sigma = F_{max}/v_c$. Four kinematic configurations used in the simulations are shown in Table 4. The simulation results are displayed in Figs. 6 and 7 and Table 4. Figure 6 shows the impact ellipsoids of different configurations. Figure 7 shows more details about the impact ellipsoids in Fig. 6. The ellipsoids are drawn in the 2D plane. Because for the planar two-link VSL robot, the out-of-plane

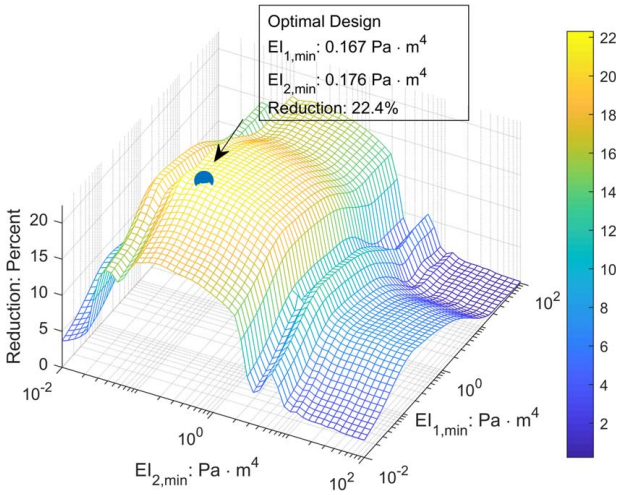

Fig. 5 Flexibility optimization result

Table 3 Design parameters used in the simulation

	Mass of the link (kg)	EI range ($\text{Pa} \cdot \text{m}^4$)
Optimal design	Link 1: 3.45 Link 2: 0.62	Link 1: [0.167, 16.7] Link 2: [0.176, 17.6]
Non-optimized	Link 1: 2.04 Link 2: 2.04	Link 1: [0.5, 50] Link 2: [0.5, 50]
Mass-optimized	Link 1: 3.45 Link 2: 0.62	Link 1: [0.5, 50] Link 2: [0.5, 50]

Table 4 Impact force reduction and maximum safe speed indices (optimal design)

Joints 2: deg	Impact force reduction $\Delta\gamma$ (%)	Max. safe speed (m^3/s^3)
#1: 0	17.34	11.54
#2: 45	23.33	22.75
#3: 90	27.12	19.24
#4: 135	27.13	16.56

Table 5 Impact force reduction and maximum safe speed indices (non-optimized design)

Joints 2: deg	Impact force reduction $\Delta\gamma$ (%)	Max. safe speed (m^3/s^3)
#1: 0	23.39	8.18
#2: 45	26.12	15.53
#3: 90	27.44	12.28
#4: 135	28.42	11.39

direction is always a singular impact direction, so the impact strength is $\sqrt{k_c m_h}$. The results for the non-optimized design and mass-optimized design are shown in Tables 5 and 6.

The impact force reductions for the four tests are close to the global impact force reduction of 22.4% in Sec. 4.4. Using the ellipsoid with the maximum flexural rigidity, the maximum safe speed can also be calculated by Eq. (31). From the four results, the impact force reduction and maximum safe speed depend on the kinematic configuration and impact direction. Even though the mass properties and flexibility are optimized by the proposed method, the impact force reduction is small in some configurations, such as the impact along the x-axis, while the angle of joint 2 is zero (see Fig. 7(*a*)). Another interesting point can be found from the results is that the impact ellipsoid always has a principal semi-axis which is nearly or completely collinear with link 2. For impact along that direction, link 2 is nearly/completely singular and it will have limited/no effect on the impact force reduction. Note that link 1 is not singular in configuration 2, 3, and 4. But link 1 is far from the end effector, and it has a smaller effect than link 2. Therefore, there is always a principal semi-axis, which is nearly/completely collinear with link 2. With this information, VS robots should avoid any impacts along the local singular direction (along link 2 for this example).

Table 6 Impact force reduction and maximum safe speed indices (mass-optimized design)

Joints 2: deg	Impact force reduction $\Delta\gamma$ (%)	Max. safe speed (m^3/s^3)
#1: 0	15.70	11.46
#2: 45	21.28	22.44
#3: 90	24.23	19.13
#4: 135	23.79	16.45

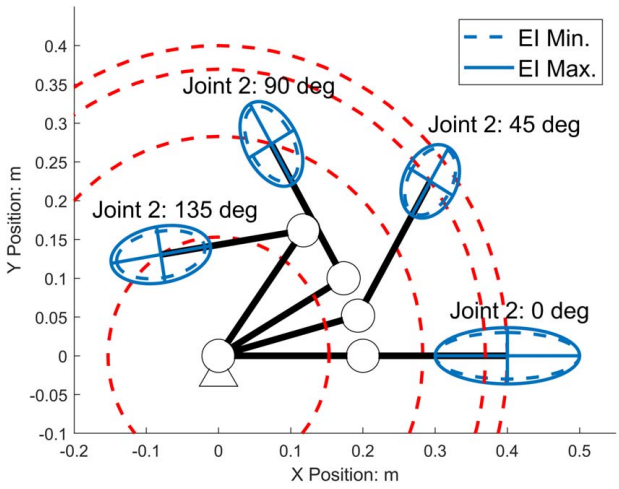

Fig. 6 Impact ellipsoids of different configurations (circle dashed lines are the reach of the robot with different configurations of joint 1)

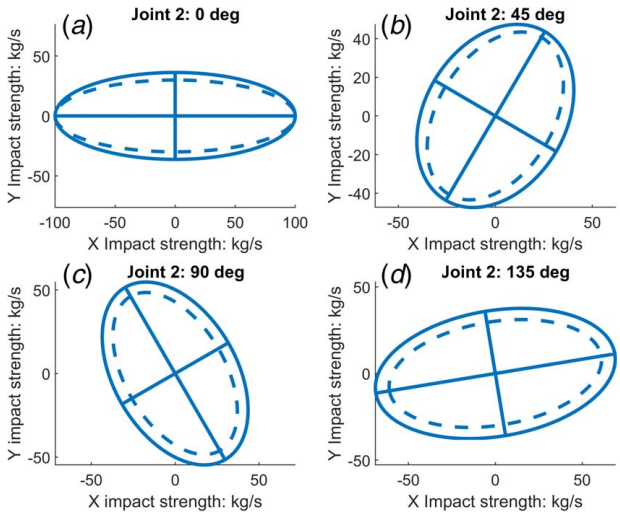

Fig. 7 Impact ellipsoids in Fig. 6 (solid: EI Max.; dashed: EI Min.). Note: (*a*) joint 2: 0 deg, (*b*) joint 2: 45 deg, (*c*) joint 2: 90 deg, and (*d*) joint 2: 135 deg.

From Table 5, compared with the optimal design, the non-optimized design has more impact force reduction but a poor performance on the maximum safe speed due to the heavyweight of link 2. Calculating the local performance by Eq. (24), the four configurations of the non-optimized design have an average local performance 0.3901 (no unit). As can be seen from Table 6, after the mass optimization, the impact force reduction decreases, while the performance on the maximum safe speed is improved. The average local performance ($\Delta\gamma + R \cdot \xi_{\max}$with $R = 0.0107$) of the mass-optimized design is 0.3983, which is also improved compared with the non-optimized design. With the full-optimization process, the impact force reduction is optimized compared with the mass-optimized design. The optimal design also has an average local performance 0.4248, which is the best among the three designs.

5 Conclusions

In this paper, we discussed a method for evaluating the impact force reduction and maximum safe speed for VS robots. Further, design optimization was proposed to optimize the global impact force reduction and maximum safe speed. In the two-link VSL example, we presented how to adjust the weighting factor $R$to compromise between the impact force reduction and maximum safe speed. It is worth mentioning that even after the optimization, the impact force reduction can still be very insignificant in some cases (with singularity). Also, the local measures of the impact force reduction and maximum safe speed are not limited to the volume of the ellipsoid, and different local measures can be used in the optimization.

Acknowledgment

The work was partially supported by NSF Award #1637656.

References

[1] "ISO10218: Robots and Robotic Devices—Safety Requirements for Industrial Robots Part 1: Robots," International Organization for Standardization, 2011.
[2] Bicchi, A., and Tonietti, G., 2004, "Fast and "Soft-Arm" Tactics [Robot Arm Design]," IEEE Rob. Autom. Mag., **11**(2), pp. 22–33.
[3] Lee, S.-D., Kim, B.-S., and Song, J.-B., 2013, "Human–Robot Collision Model With Effective Mass and Manipulability for Design of a Spatial Manipulator," Adv. Rob., **27**(3), pp. 189–198.
[4] She, Y., Su, H.-J., Meng, D., Song, S., and Wang, J., 2018, "Design and Modeling of a Compliant Link for Inherently Safe Corobots," ASME J. Mech. Rob., **10**(1), p. 011001.
[5] Albu-Schäffer, A., Ott, C., and Hirzinger, G., 2007, "A Unified Passivity-Based Control Framework for Position, Torque and Impedance Control of Flexible Joint Robots," Int. J. Rob. Res., **26**(1), pp. 23–39.
[6] Haddadin, S., Albu-Schaffer, A., Luca, A. D., and Hirzinger, G., 2008, "Collision Detection and Reaction: A Contribution to Safe Physical Human-Robot Interaction," 2008 IEEE/RSJ International Conference on Intelligent Robots and Systems, Nice, France, Sept. 22–26.
[7] Song, S., She, Y., Wang, J., and Su, H., 2018, "Barrier Lyapunov Function Based Control of a Flexible Link Co-Robot With Safety Constraints," ASME 2018 Dynamic Systems and Control Conference, Atlanta, GA, Nov. 12.
[8] Ferraguti, F., Landi, C. T., Sabattini, L., Bonfe, M., Fantuzzi, C., and Secchi, C., 2019, "A Variable Admittance Control Strategy for Stable Physical Human–Robot Interaction," Int. J. Rob. Res., **38**(6), pp. 747–765.
[9] Song, S., Zeng, X., She, Y., Wang, J., and Su, H.-J., 2019, "Modeling and Control of Inherently Safe Robots With Variable Stiffness Links," Rob. Auton. Syst., **120**, p. 103247.
[10] Kulić, D., and Croft, E., 2005, "Safe Planning for Human-Robot Interaction," J. Rob. Syst., **22**(7), pp. 383–396.
[11] Sisbot, E. A., Marin-Urias, L. F., Alami, R., and Simeon, T., 2007, "A Human Aware Mobile Robot Motion Planner," IEEE Trans. Rob., **23**(5), pp. 874–833.
[12] Hong, S., Cho, C., Lee, H., Kang, S., and Lee, W., 2017, "Joint Configuration for Physically Safe Human–Robot Interaction of Serial-Chain Manipulators," Mech. Mach. Theory, **107**, pp. 246–260.
[13] Haddadin, S., Albu-Schäffe, A., and Hirzinger, G., 2009, "Requirements for Safe Robots: Measurements, Analysis and New Insights," Int. J. Rob. Res., **28**(11–12), pp. 1507–1527.
[14] Tonietti, G., Schiavi, R., and Bicchi, A., 2005, "Design and Control of a Variable Stiffness Actuator for Safe and Fast Physical Human/Robot Interaction," Proceedings of the 2005 IEEE International Conference on Robotics and Automation, Barcelona, Spain, Apr. 18–22 .
[15] Schiavi, R., Grioli, G., Sen, S., and Bicchi, A., 2008, "VSA-II: A Novel Prototype of Variable Stiffness Actuator for Safe and Performing Robots Interacting With Humans," 2008 IEEE International Conference on Robotics and Automation, Pasadena, CA, May 19–23 .
[16] Stilli, A., Wurdemann, H., and Althoefer, K., 2017, "A Novel Concept for Safe, Stiffness-Controllable Robot Links," Soft Rob., **4**(1), pp. 16–22.
[17] Stilli, A., Grattarola, L., Feldmann, H., Wurdemann, H. A., and Althoefer, K., 2017, "Variable Stiffness Link (VSL): Toward Inherently Safe Robotic Manipulators," 2017 IEEE International Conference on Robotics and Automation, Singapore, May 29–June 3.
[18] Hao, L., Xiang, C., Giannaccini, M. E., Cheng, H., Zhang, Y., Nefti-Meziani, S., and Davis, S., 2018, "Design and Control of a Novel Variable Stiffness Soft Arm," Adv. Rob., **32**(11), pp. 605–622.
[19] Zhou, Y., Headings, L. M., and Dapino, M. J., 2019, "Discrete Layer Jamming for Variable Stiffness Co-Robot Arms," ASME J. Mech. Rob., **12**(1), p. 015001.
[20] She, Y., 2018, *Compliant Robotic Arms for Inherently Safe Physical Human-Robot Interaction*, The Ohio State University, Columbus, OH.
[21] Walker, I., 1994, "Impact Configurations and Measures for Kinematically Redundant and Multiple Armed Robot Systems," IEEE Trans. Rob. Autom., **10**(5), pp. 670–683.
[22] Hu, J., and Wang, T., 2017, "Pre-Impact Configuration Designing of a Robot Manipulator for Impact Minimization," ASME J. Mech. Rob., **9**(3), p. 031010.
[23] Patel, S., and Sobh, T., 2015, "Manipulator Performance Measures—A Comprehensive Literature Survey," J. Intell. Rob. Syst., **77**(3–4), pp. 547–570.
[24] Gosselin, C., and Angeles, J., 1991, "A Global Performance Index for the Kinematic Optimization of Robotic Manipulators," ASME J. Mech. Des., **113**(3), pp. 220–226.
[25] Gao, D., and Wampler, C. W., 2009, "Head Injury Criterion," IEEE Rob. Autom. Mag., **16**(4), pp. 71–74.
[26] Newman, J. A., Shewchenko, N., and Welbourne, E., 2000, "A Proposed New Biomechanical Head Injury Assessment Function—The Maximum Power Index," Stapp Car Crash J., **44**, p. 362.
[27] Gadd, C., 1966, "Use of Weighted Impulse Criterion for Estimating Injury Hazard," 10th Stapp Car Crash Conference, New York, Feb. 1.
[28] Haddadin, S., 2014, *Towards Safe Robots: Approaching Asimov's 1st Law*, Springer, Berlin.
[29] Spong, M., and Vidyasagar, M., 1989, *Robot Dynamics and Control*, John Wiley & Sons, New York.
[30] Khatib, O., 1995, "Inertial Properties in Robotic Manipulation: An Object-Level Framework," Int. J. Rob. Res., **13**(1), pp. 19–36.
[31] Spong, M., 1987, "Modeling and Control of Elastic Joint Robots," J. Dyn. Syst. Meas. Control, **109**(4), pp. 310–318.
[32] DeLuca, A., and Siciliano, B., 1989, "Trajectory Control of a Non-Linear One-Link Flexible Arm," Int. J. Control, **50**(5), pp. 1699–1715.
[33] Tso, S. K., Yang, T., Xu, W., and Sun, Z., 2003, "Vibration Control for a Flexible-Link Robot Arm With Deflection Feedback," Int. J. Non-Linear Mech., **38**(1), pp. 51–62.
[34] Jafari, A., Tsagarakis, N. G., Sardellitti, I., and Caldwell, D. G., 2014, "A New Actuator With Adjustable Stiffness Based on a Variable Ratio Lever Mechanism," IEEE/ASME Trans. Mechatronics, **19**(1), pp. 55–62.
[35] Shin, H., and Choi, S., 2001, "Position Control of a Two-Link Flexible Manipulator Featuring Piezoelectric Actuators and Sensors," Mechatronics, **11**(6), pp. 707–729.
[36] Wit, C. C. d., Siciliano, B., and Bastin, G., 2012, *Theory of Robot Control*, Springer, New York.
[37] Dempste, W., and Gaughran, G., 1967, "Properties of Body Segments Based on Size and Weight," Am. J. Anat., **120**(1), pp. 33–54.
[38] "ISO/TS 15066:2016 Robots and Robotic Devices—Collaborative Robots," International Organization for Standardization, 2016.
[39] She, Y., Meng, D., Shi, H., and Su, H.-J., 2015, "Dynamic Modeling of a 2D Compliant Link for Safety Evaluation in Human-Robot Interactions," 2015 IEEE/RSJ International Conference on Intelligent Robots and Systems, Hamburg, Germany, Sept. 28–Oct. 2.
[40] Morrison, T., Li, C., Pei, X., and Su, H.-J., 2019, "A Novel Rotating Beam Link for Variable Stiffness Robotic Arms," 2019 International Conference on Robotics and Automation (ICRA), Montreal, Canada, May 20–24.